The Effect of VSC HVDC Control on AC System Electromechanical Oscillations and DC System Dynamics

L. Shen, *Student Member, IEEE*, M. Barnes, *Senior Member, IEEE*, R. Preece, *Member, IEEE,* Jovica V. Milanović, *Fellow, IEEE*, K.R.W. Bell, *Member, IEEE,* and M. Belivanis

***Abstract*-- In order to strengthen the onshore transmission network in many parts of the world, VSC HVDC will increasingly be utilized. The effect of the operating point of a VSC HVDC link and the control strategies employed can substantially affect the electromechanical oscillatory behavior of the AC network as well as the DC side dynamics. In order that the full, flexible capability of VSC HVDC can be exploited, further study of the effects of these controllers and their interactions with AC system responses is necessary. This paper addresses this gap. Both modal analysis and transient stability analysis are used to highlight tradeoffs between candidate VSC-HVDC power controllers and to study the electromechanical performance of the integrated AC/DC model. Tests are carried out on both a generic two-area model and a large-scale realistic network with detailed AC generator and HVDC models.**

***Index Terms*-- VSC HVDC control, Electromechanical modes, Modal Analysis, Inter-area oscillation.**

I. Introduction

Voltage-Source Converter High-Voltage DC Transmission (VSC HVDC) technology has evolved to the point where it is considered the main candidate for the connection of large renewable energy sources located far-offshore [1]. It is also a leading candidate for the reinforcement of onshore networks through use of underground or undersea cable links. This is likely to result in its wide-spread proliferation in integrated AC/DC systems. Many challenges remain before the potential impact of this change to system architecture is thoroughly understood.

A great deal of excellent research on this problem has been undertaken but approaches have tended to view the problem with an emphasis on either the AC network or the DC network, with consequent simplifications of the other side. A holistic approach needs to be taken. This paper uses a detailed AC/DC modeling methodology and control designs to systematically compare candidate VSC-HVDC controllers. Their effects on the electromechanical oscillatory behavior of the AC network and DC system dynamics have not been systematically studied in the past and therefore a thorough comparison is necessary. In this respect this paper presents both, a novel methodology for controller analysis and a new set of recommendations for controller configuration.

VSCs have complex hierarchical control structures. A variety of these have been proposed and analyzed [2-6] but the focus has been the delivery of required performance on the DC side and within the converter rather than the interaction with the AC system. The AC system has thus not been modeled in detail in these cases. Conclusions have been reached about the efficacy of droop control [2] used in multi-terminal DC grids and supplementary power oscillation damping (POD) controllers [7]. AC system studies have also been undertaken but the focus has been on the AC system dynamics - the VSC-HVDC system and controllers have typically been severely abstracted [7, 8]. This paper reinforces this research by a systematic comparison using a system with full detailed models of AC and DC system components.

In this paper the effect of VSC HVDC control and operating condition are addressed by studying: (1) effects on AC system inter-area oscillation and (2) effects on DC system dynamic responses. The analysis is focused on the case of a point-to-point DC link embedded within each of two test AC systems. One is the commonly studied two-area system designed for inter-area electromechanical oscillation analysis [9]. This facilitates analysis of the effects of VSC HVDC without being obscured by complex AC system structures. The second AC test network is a dynamic equivalent representation of a Great Britain (GB) like transmission network as initially described in [10] and defined in [11] with the intention of reproducing realistic responses and power flow constraints without over-burdening researchers with excessive detail in the course of study of new concepts. The use of a realistic large power system model with realistic constraints and reinforcement strategies facilitates practicality of the studies carried out and generalization of conclusions.

II. VSC Model and Control Schemes

A. Inner Loop

The control system for VSC has a hierarchical cascaded structure which can be classified into 3 levels (L1- L3 in Fig.1) with appropriate bandwidth separation. Due to the phenomenon considered in this study the focus is on analysis

Manuscript for IEEE transactions on Power Delivery. This work was supported by National Grid and by the Research Councils UK, through the HubNet consortium (grant number: EP/I013636/1).

L.Shen, M.Barnes, J.V.Milanović and R.Preece are with School of Electrical and Electronic Engineering, The University of Manchester, Manchester M13 9PL(e-mail: seevy.shen@gmial.com).

K.R.W Bell and M. Belivanis, are with the Department of Electronic and Electrical Engineering at the University of Strathclyde, Glasgow.

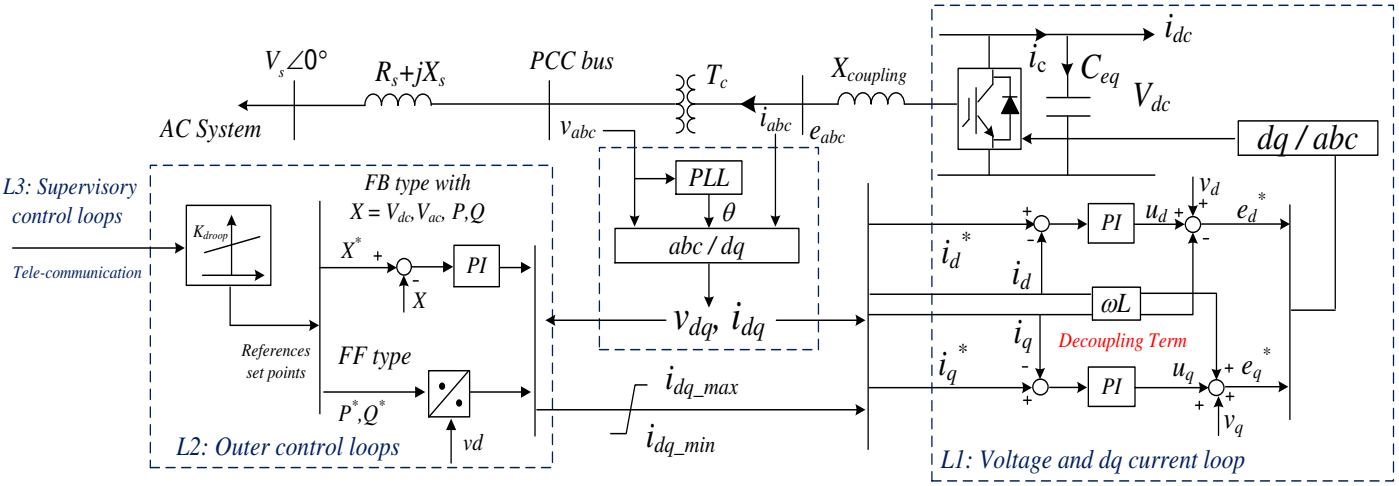

Fig.1. Full diagram of VSC terminal model and control structure.

of the influence of outer controllers (L2) only, as illustrated in Fig 1. The fast inner loop (L1) includes the DC to AC voltage conversion and a decoupled vector current control (*dq* current control). Typically, a Phase Locked Loop (PLL) is employed to lock on to the Point of Common Coupling (PCC) voltage and provide the reference angle for the VSC.

B. Outer Voltage and Power Loops

Based upon the fast inner loop, different cascaded outer control loops (L2 in Fig.1) can be added. These options can be categorized as feed forward (FF) and feedback (FB) types which are briefly summarized as:

1. FB DC voltage control (FBV_{dc}) [3, 4] - maintains constant DC voltage for the VSCs and requires the measurement of DC link voltage as a feedback, typically through a proportional-integral (PI) controller.

2-3. FF real and reactive power control (*FFP and FFQ*) [12] - controls the converter power to the reference values. This in principle has the potential for fast response to converter power variations but may be affected when the PLL is inaccurate during fault or unbalanced conditions [5].

4-5. FB real and reactive power control (*FBP and FBQ*) [3, 13-15] - adds an additional power controller loop, potentially complicating controller design. However, the control is then less sensitive to PCC voltage variations and hence may be more stable for practical implementation.

6. FB AC voltage control (FBV_{ac}) [4, 6] - regulates AC side voltage and may be preferred in situations where a grid connected VSC would provide support to improve the AC network dynamic performance.

7. DC voltage droop control (*droop*) [2] - includes an additional droop gain (k_{droop}) to relate DC side voltage to power orders. It is especially useful in multi-terminal DC grid operation as there can be multiple converters participating in DC voltage control simultaneously. The droop gain can be either added to FF or FB type power controls (2-5).

For convenience, the above abbreviations for the outer control schemes will be used in the following text.

III. Control Parameterization

The closed loop *bandwidth* of the VSC outer control loops refers to the frequency where the magnitude of the response is equal to -3dB. Normally, the *bandwidth* falls into the range of a few Hz to tens of Hz (e.g. 1-20Hz). It is therefore possible that these controllers will influence the electromechanical behaviors of the connected AC system. In this section, the parameterization of these outer controllers will be discussed. To complete this, it is assumed that the inner current loops are fast enough to be simplified as constant gains and the AC system dynamics are considered as infinite buses. The notations defined in Fig.1 will be used in this section.

With power invariant *dq* transformation and the assumption that the rotating reference frame is aligned to the d-axis, the VSC output power at the PCC bus can be expressed as:

$$p = v_d i_d + v_q i_q \approx v_d i_d \tag{1}$$

$$q = v_q i_d - v_d i_q \approx -v_d i_q \tag{2}$$

where v_{dq} and i_{dq} are the voltage and current at the PCC bus. These equations are used by *FFP* and *FFQ* which relate directly the real and reactive power orders to *dq* current orders and therefore no additional outer controllers are introduced. The block diagram representations of the feedforward type PQ controls are presented in Fig.2.

Droop control adds an additional gain to the FF or FB power loops which set the allowable DC voltage variations for given power limitations. To cover the typical droop gains, the range of $1 < k_{droop} \leq 30$ will be considered in this paper [2].

With respect to the four FB type outer control loops with additional PI controllers (i.e. FBV_{dc}, *FBP, FBQ,* FBV_{ac}), the parameter settings can be determined by means of frequency responses of closed loop transfer functions.

A. Modelling of Feedback DC Voltage Loop

The dynamics of the FBV_{dc} controller are dominated by the DC side capacitor and are expressed as:

$$C_{eq}\frac{dV_{dc}}{dt} = i_c - i_{dc} = \frac{v_d i_d}{V_{dc}} - i_{dc}. \tag{3}$$

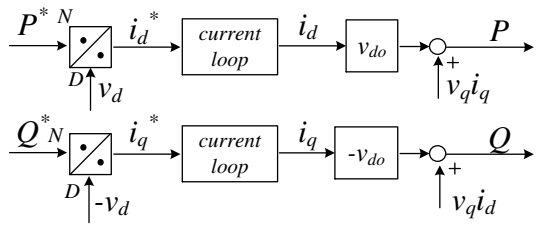

Fig.2 VSC FF type control block diagram representations.

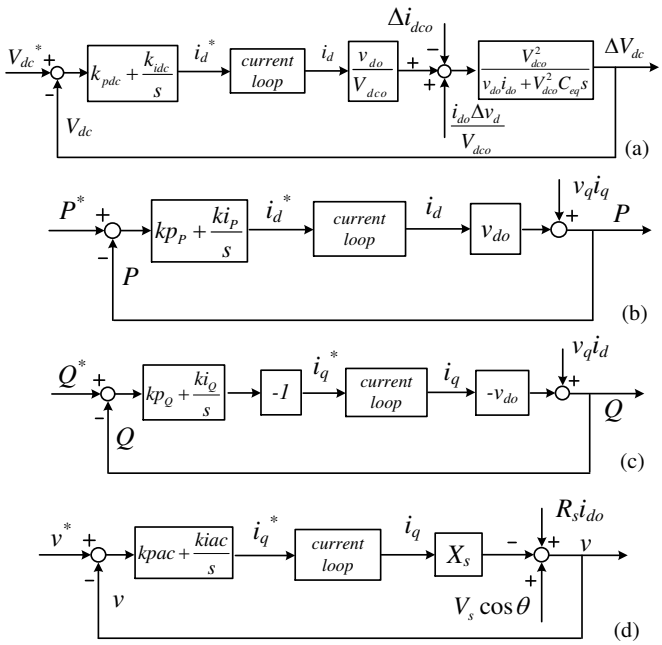

Fig. 3. VSC FB type control block diagram representations.

Linearizing gives:

$$\Delta C_{eq} \frac{dV_{dc}}{dt} = -\frac{v_{do} i_{do}}{V_{dco}^2} \Delta V_{dc} + \frac{v_{do}}{V_{dco}} \Delta i_d + \frac{i_{do}}{V_{dco}} \Delta v_d - \Delta i_{dc} \tag{4}$$

where a subscript 'o' represents the operating point value. Based on the above equation, the closed control loop can be represented by Fig.3(a). Let $K_v = v_{do}/V_{dco}$ and $K_G = i_{do}/V_{dco}$, the closed loop transfer function is expressed as:

$$\frac{V_{dc}}{V_{dc}^*} = \frac{k_{pdc} K_V s + k_{idc} K_V}{C_{eq} s^2 + (K_V K_G + k_{pdc} K_V) s + k_{idc} K_V}. \tag{5}$$

This equation can be further approximated to a second order transfer function (assuming $k_{pdc} \ll k_{idc}$) as:

$$\frac{V_{dc}}{V_{dc}^*} = \frac{\frac{k_{idc} K_V}{C_{eq}}}{s^2 + \frac{K_V (K_G + k_{pdc})}{C_{eq}} s + \frac{k_{idc} K_V}{C_{eq}}} = \frac{\omega_n^2}{s^2 + 2\xi_{dc} \omega_n s + \omega_n^2}. \tag{6}$$

This allows an approximation of an initial tuning value for the controller for a given natural undamped frequency ω_n and damping ratio ξ_{dc}.

B. Modelling of Feedback Real and Reactive Loop

Based on equations (1) and (2), the closed FB real and reactive power control loops can be defined as Fig.3(b-c)

Ignoring the disturbance terms, the plant model for both real and reactive power is mainly determined by the operating point PCC voltage $\pm v_{do}$, which can be represented by a gain g at an operating point and then the closed loop transfer function for both *FBP* and *FBQ* takes the form of a first order transfer function as (assuming $k_{pPQ} \ll k_{iPQ}$):

$$\frac{x}{x^*} = \frac{g k_{pPQ} s + k_{iPQ}}{s + g k_{pPQ} s + k_{iPQ}} \approx \frac{k_{iPQ}}{s + k_{iPQ}} \quad (g = \pm v_{do}) \tag{7}$$

where x can be either P or Q. The target *bandwidth* can be initially approximated by k_{iPQ}.

C. Modelling of Feedback AC Voltage Loop

For the FB type AC voltage control, the closed loop transfer function derivation is slightly more involved. Assuming an infinite AC bus with voltage $Vs\angle 0°$ (Fig.1), after *dq* transformation, the following equations was established:

$$(v_d + jv_q) - (V_{sd} + jV_{sq}) = (R_s + jX_s)(i_d + ji_q). \tag{8}$$

Solving gives:

$$\begin{aligned} v_d &= V_{sd} + R_s i_d - X_s i_q \\ v_q &= V_{sq} + R_s i_q + X_s i_d. \end{aligned} \tag{9}$$

For an ideal PLL, the PLL angle will vary with the PCC bus voltage angle, and so are all other system parameters in the *dq* domain. The infinite bus voltage $V_s\angle 0°$ in the *dq* domain is:

$$\begin{bmatrix} V_{sd} \\ V_{sq} \end{bmatrix} = \begin{bmatrix} \cos\theta & \sin\theta \\ -\sin\theta & \cos\theta \end{bmatrix} \begin{bmatrix} V_{sr} \\ V_{si} \end{bmatrix} \tag{10}$$

where $V_{si}=0$ and $V_{sr}=V_s$. θ is the PLL angle.

With equations (9) and (10), and the rotating reference frame being aligned with the d-axis (i.e. $v_q=0$), the PCC bus voltage is now given as:

$$v = \sqrt{v_d^2 + v_q^2} \approx v_d = V_s \cos\theta + R_s i_d - X_s i_q. \tag{11}$$

The closed loop transfer function for FBV_{ac} can then be expressed as Fig.3(d) which is disturbed by $R_s i_{do}$ (related to the operating point of the DC link) and $V_s cos\theta$. The closed loop transfer function is, however, similar to equation (7) where the *bandwidth* can be initially approximated by k_{iac}.

The above simplified control closed loop transfer functions of the four FB type controls allow quick tuning of the controllers, after the initial approximation, to achieve a given closed loop bandwidth. More accurate controller parameters can be further set by examining the frequency responses of the closed loop transfer functions via Matlab software (Matlab pidtool) with the tuning techniques outlined in [16]. For each FB type control loop, a set of parameters is tuned for the outer controllers to cover their typical *bandwidth* range in preparation for comparison purposes in the later stages.

IV. Method of Analysis

This section introduces the techniques that are used to analyze the effect of VSC controls and operating points. The influence brought by the control strategies on the AC and DC side of the system are investigated separately with different methodologies.

A. Effects on AC System

From the perspective of the AC side, the investigation focuses on the impact of VSC HVDC link on inter-area electromechanical modes in the AC system. In order to

identify the critical oscillatory modes, the eigenvalues of the system with frequencies in the range of 0.2 to 1 Hz need to be scanned. Two modal analysis techniques are used: (1) the QR method [17] which is robust for small power systems and (2) the Arnoldi method [18] that can be implemented with sparsity techniques to calculate a specific set of eigenvalues with certain features of interest (e.g. the low frequency inter-area modes in this case). The Arnoldi method is considered efficient to solve partial eigenvalues for large integrated AC/DC systems. The application of this sparsity based eigenvalue technique to the small disturbance stability analysis of a large power system was presented in [19]. Mode shape (given by the right eigenvector of state matrix A) is calculated to demonstrate the relative activity of the state variables [9] in critical system modes.

As AC system inter-area oscillations are complex and involve a large number of generators, a generic small two-area system with a characteristic inter-area mode is firstly investigated. The QR method is used to track the critical oscillatory mode for this small system. The key findings are then tested with a larger and more realistic representative GB system where the Arnoldi method is applied for inter-area mode monitoring.

B. Effects on DC System

The dynamic responses in the DC side of the system are much faster than those in the AC side. Hence the effects of VSC controls on the DC system are less influenced by the AC side dynamics and are better shown by DC side transient responses. Therefore, the controls are compared by monitoring the dynamic responses of DC system parameters. Different controller parameter settings, based on the tuning procedures in Section III, are applied to provide a sensitivity analysis showing the resulting system behaviors.

The main focus of this paper is on normal operating conditions and thus the test conditions modelled do not cause control limiters to be activated.

V. Investigation Based on Generic AC System

The classical two-area AC system from [9] is firstly used in these studies with approximately 400MW power transfer from Area1 to Area2 (Fig.4). A point to point VSC HVDC link is connected in parallel with the AC tie lines sharing the power transferred between the two areas in the same direction. This is a detailed integrated AC/DC system with 6th order generator models and VSC models with control schemes shown in Fig.1. Details of the generator controls and network information are given in [9]. The VSC HVDC model is developed based on [6], [20] which is suitable for small signal stability analysis. The key state equations as well as some important parameters used in this point-to-point VSC HVDC link model are provided in Appendix.

In the following studies, the term “fast” and “slow” controls will be used to represent a FB type control which is tuned with a *bandwidth* of 30Hz and 1Hz respectively. The purpose for this is to push a particular controller to its parameter setting limits to show the corresponding effects under certain conditions.

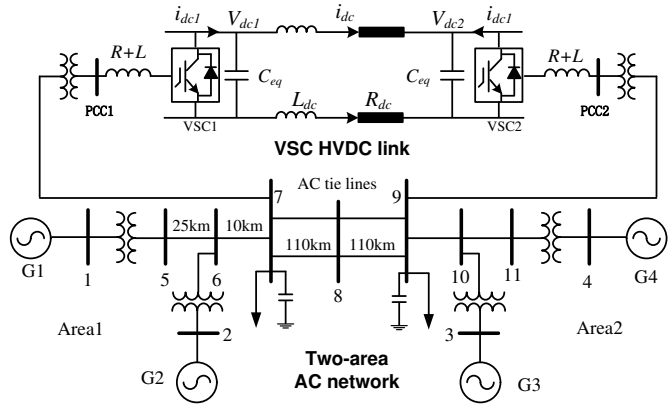

Fig. 4. Generic two-area system with embedded VSC HVDC link.

A. Effects of VSC Outer Controls on Inter-area Mode

The idea here is to investigate the AC system inter-area oscillation under the effect of different VSC outer control schemes and operating points. Specifically, the AC system low frequency inter-area mode is monitored by applying QR method to the whole system matrix with different VSC HVDC configurations. However, for FB type controllers, as they can be configured differently depending on the outer controller, the investigation of their effects needs to cover their typical settings. This is achieved by including a *bandwidth* sensitivity analysis for each of these FB controls detailed in test case 2.

1) Test Case 1: Comparison of FF and FB type controls

Two control scenarios are listed in Table I where FBV_{dc} is configured to a *bandwidth* of 10Hz in both cases.

The FF type PQ controls in Scenario 1 which do not require additional controllers are examined first. The QR method is applied to obtain the inter-area mode for different power flow conditions in the DC link. The resulting inter-area mode frequencies (f) and damping ratios (ξ) are listed in Table II.

All the FF type PQ controls in Table I are replaced by FB type PQ controls (Scenario 2) with identical bandwidths. The same test now yields results shown in Table III.

Originally, without the embedded DC link, the two-area system has an inter-area mode of $f=0.545Hz$ and $\xi=3.2\%$ [9]. According to the results in Table II, it is seen that the inter-area mode damping ratio increases with the DC link power when FF type PQ controls are employed. In contrast, adding the DC link with FB type PQ controls (Table III), the inter-area mode damping ratio decreases with the DC link power. In both cases the frequency of the mode remains largely the same. A faster or slower FB type PQ controller does not influence significantly the inter-area mode. This is validated by a time domain simulation in Fig.5 by comparing the tie line power responses for both scenarios with different DC link powers following a three phase 100ms self-clearing fault at bus5.

2) Test Case 2: Effects of individual FB type controls

Case 2 focuses on individual FB type control schemes. In setting up the comparison of various control parameters in this case study, a reference base case is firstly defined. The DC link is now configured with a control strategy specified in Table IV, i.e., all the FB control loops are tuned to have a *bandwidth* of 5Hz except FBV_{dc} which is tuned to 10Hz. This

Table I VSC control settings case 1

Control Scenarios	VSC1		VSC2	
Scenario 1	*FBV_{dc}*	*FFQ*	*FFP*	*FFQ*
Scenario 2	*FBV_{dc}*	*FBQ*	*FBP*	*FBQ*

Table II Inter-area mode tracking with FF type controls

DC link power	Inter-area mode	
	f Hz	*ξ %*
50MW	*0.56Hz*	*3.82%*
150MW	*0.56Hz*	*4.54%*
250MW	*0.56Hz*	*5.25%*
350MW	*0.55Hz*	*5.86%*

Table III Inter-area mode tracking with FB type controls

DC power	Inter-area mode			
	Slow FB controls		Fast FB controls	
	f Hz	*ξ %*	Frequency	*ξ %*
50MW	*0.56Hz*	*3.45*	*0.57Hz*	*3.48*
150MW	*0.58Hz*	*3.32*	*0.58Hz*	*3.36*
250MW	*0.58Hz*	*3.07*	*0.58Hz*	*3.10*
350MW	*0.57Hz*	*2.66*	*0.57Hz*	*2.66*

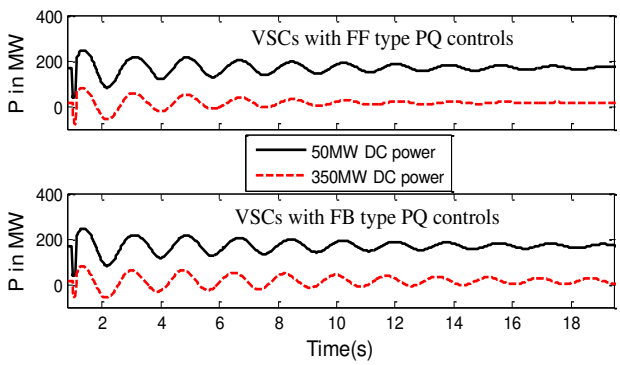

Fig. 5. Tie line power responses at different operating points.

Table IV VSC control settings case 2

VSC1		VSC2	
FBV_{dc}	*FBQ/FBV_{ac}*	*FBP*	*FBQ/FBV_{ac}*

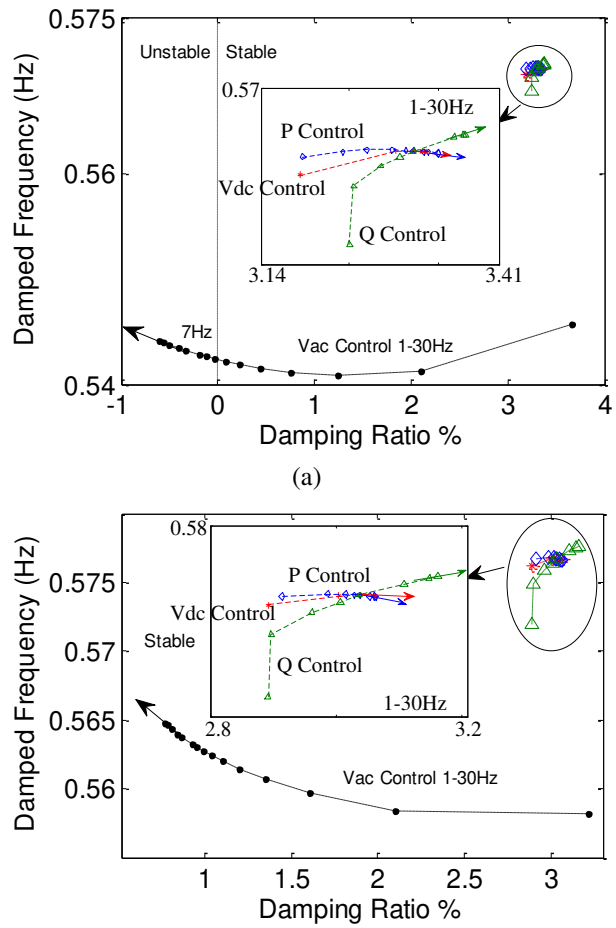

Fig. 6. Root loci of inter-area mode with bandwidth variations in individual FB type control loop at (a) 100MW DC link power and (b) 200MW DC link power.

serves as a reference case so that the resulting closed loop step responses for these FB type controls have no significant overshoot, have 10%-90% rise time of 0.1s and no steady state error.

The *FBQ* in VSC2 was changed to FBV_{ac} when analyzing the effect of AC voltage control. The procedure of the bandwidth sensitivity analysis is a set of iterative processes where one controller will be varied with different *bandwidth*s by adjusting the outer loop PI controller each time while all the other controllers in the DC link remain at the settings of the reference case. In this case, FBV_{dc} in VSC1, *FBP*, *FBQ* or FBV_{ac} in VSC2 is varied for testing.

For two DC link operating points, the root loci of the inter-area mode, which is affected by different control settings, are plotted in Fig.6(a-b) with arrows indicating the directions of increasing controller *bandwidth*. The *bandwidth*s of the controllers here are pushed to a larger range (1-30Hz) to more clearly show the movement of the inter-area mode.

The results, illustrated by Fig.6(a-b) for 100MW and 200MW DC link power flow conditions respectively, lead to the following conclusions:

2a. The inter-area mode damping ratio increases with the *bandwidth* of FBV_{dc}, *FBP* and *FBQ*. However, such an impact is very small relative to the effect of the *bandwidth* variations in FBV_{ac}.

2b. *FBQ* has a larger impact on the inter-area mode damping ratio and frequency when the DC link operating point is higher.

2c. The inter-area mode damping deteriorates as the *bandwidth* is increased for FBV_{ac} in VSC2. This is particularly true for the case of 100MW DC link power, when the damping ratio of the inter-area mode is pushed to a negative value with a FBV_{ac} of *bandwidth* 7Hz. In such a case, the system will become unstable.

2d. The frequency of the inter-area mode is decreased when FBV_{ac} is employed in VSC2 instead of *FBQ*. However, variations in FBV_{ac} control settings have little impact on the inter-area mode frequency.

3) Test Case 3: Further investigation on FBV_{ac}

Since it was identified in test case 2 that the *bandwidth* of the AC voltage controller has the largest influence on the inter-area mode compared with all other FB type controls, this test case was analyzed further.

It can be observed from the two plots in Fig.6 that with higher DC link operating conditions, FBV_{ac} has decreased influence on the damping ratio but increased influence on the frequency of the inter-area mode. This is more clearly shown in Fig.7 which compares the inter-area mode movement affected by FBV_{ac} (*bandwidth =1-30Hz*) with respect to different DC link operating points. Other tests show that the effect of FBV_{ac} on the damping of inter-area mode also depends on its location. This is demonstrated by comparing the effect of FBV_{ac} (*bandwidth =1-30Hz*) in VSC1 (sending end) and VSC2 (receiving end) of 100MW DC link power in Fig.8.

The effect of FBV_{ac} in VSC terminals on inter-area mode is comparable to the effect of fast exciters in the synchronous generators [21]. Continuing with the conclusions in the previous test cases, some characteristics of the FBV_{ac} control can be summarized as:

3a. With an increasing DC link power, the impact of FBV_{ac} on the damping ratio of the inter-area mode decreases while the impact on the frequency of the inter-area mode increases as shown in Fig.7.

3b. The location of the FBV_{ac} has a strong impact on the damping ratio of the inter-area mode which is similar to the effect of one fast exciter in one of the four generators stated in [21]. A fast FBV_{ac} at the receiving area (VSC2) reduces the damping of the inter-area mode while one at the sending area (VSC1) improves the damping (Fig.8). This general behavior agrees to a certain extent with the case of one fast exciter and three slow exciters in the four generator test system of [21]. However, in [21], it is stated that in the case of one fast exciter and three manually controlled exciters, a fast exciter in the receiving area improves the damping while one in the send area reduces the damping. This is not the case with FBV_{ac} as further tests showed that the effect of the location of FBV_{ac} does not change when the slow exciters in the generators are replaced by manually controlled exciters.

3c. The impact of the location of FBV_{ac} on the frequency of the inter-area mode is similar to the effect of one fast exciter in one of the generators [21] - a fast FBV_{ac}/exciter in the sending area increases the frequency of the mode while one in the receiving area reduces it.

The effect of FBV_{ac} is validated by time domain simulations presented in Fig.9 which compares the tie line power responses for a three phase 100ms self-clearing fault at bus5 considering different configurations of FBV_{ac}.

Tests regarding the effect of droop gain settings on the inter-area mode are also carried out. However, in the case of a point to point DC link, different droop gains added to either FF or FB type outer controllers result in very similar inter-area mode behavior as the cases without adding the droop gain. Therefore these results have been omitted for brevity.

B. DC System Effects

The effects of VSC controls on the DC side system are reviewed by means of sensitivity analysis based on a set of simulation comparisons. In this case, the focus is put on the dynamic behaviors of the DC side voltage and the DC link real and reactive power output, when they are affected by different VSC controls. The dynamic performance of the control schemes is compared for both parameter step change events

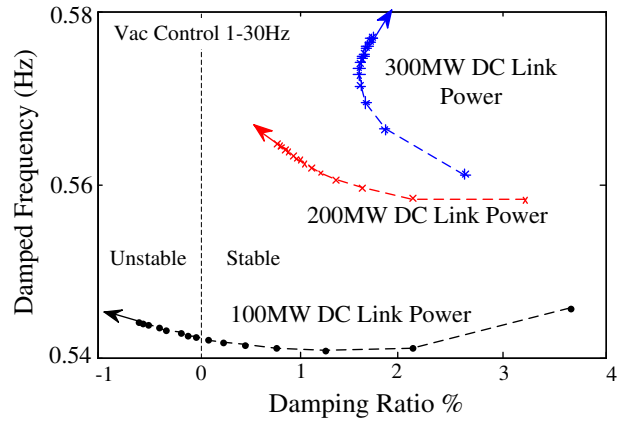

Fig 7. Root loci of the inter-area mode for FBV_{ac} Control.

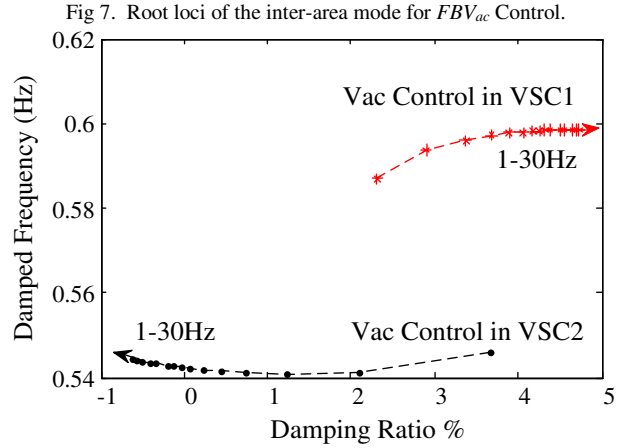

Fig. 8. Root loci of the inter-area mode for FBV_{ac} at different locations (DC link power =100MW).

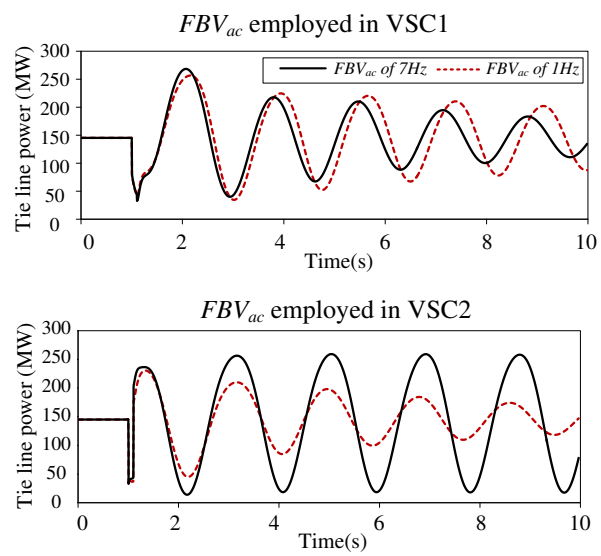

Fig. 9. Effect of FBV_{ac} control in different locations (DC link power =100MW).

and the three phase fault (same type and location of the fault as before). The results are presented in Fig.10 where (a)-(d) show the step responses and (e)-(h) show the AC fault responses. From this comparison, the following conclusions can be drawn:

1) DC side voltage

The dynamic behavior of DC link voltage is mainly affected by FBV_{dc} or droop control. Other controls (2-6 in section II)

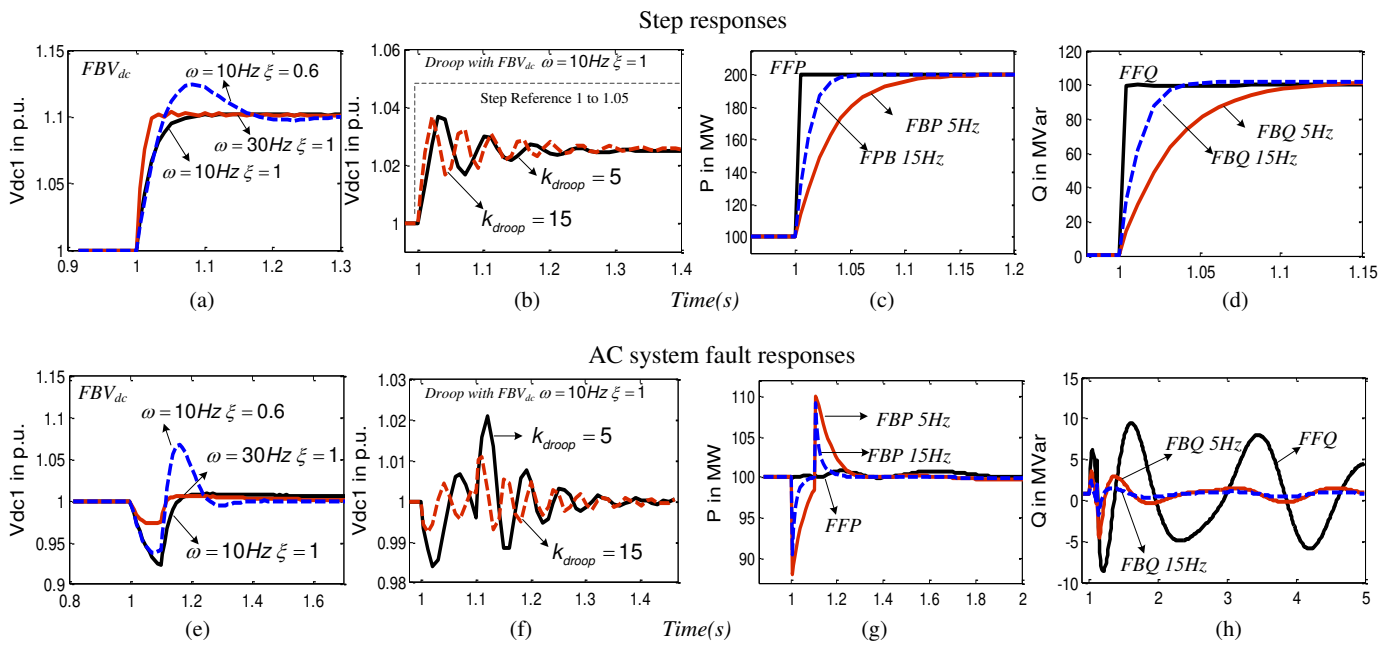

Fig. 10. DC side dynamic response comparison of different control schemes for step change (a-d) and AC system fault (e-h) events.

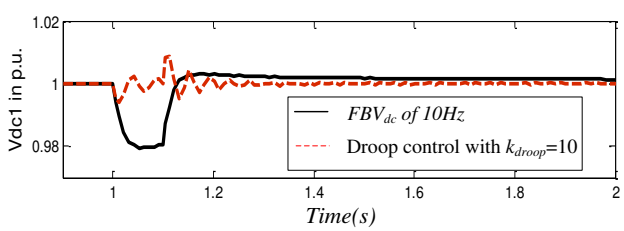

Fig. 11. Comparison of constant V_{dc} and droop control.

show limited impact on the DC voltage responses. Effects of FBV_{dc} configuration are illustrated by Fig.10(a) and Fig.10(e).

The effect of droop gain is shown in Fig.10(b) and Fig.10(f). Steady state error is seen with droop control for step changes. Larger droop gain results in slightly smaller DC voltage oscillations following the AC fault. A comparison of FBV_{dc} (*bandwidth =10Hz*) and droop control with droop gain of 10 cascaded on a *FBP* with *bandwidth =10Hz* is given in Fig.11 where droop control gives better voltage control under the AC fault.

2) *Real Power and Reactive Power*

The DC link real and reactive power outputs are mainly affected by PQ controls (2-5 in Section II). This is illustrated by Fig.10(c) and Fig.10(g) for real power responses and Fig.10(d) and Fig.10(h) for reactive power responses.

Note that, in Fig.10(h), during the AC system fault, *FFQ* results in large oscillations. This is due to the errors in PLL causing v_q to be non-zero during an AC system fault and thus the disturbance terms $v_q i_q$ and $v_q i_d$ in Fig.2 and Fig.3 are no longer zero. However, as $v_q i_q$ ($i_q \approx 0$) is much smaller than $v_q i_d$, larger oscillations appear with *FFQ* control for the AC system fault event. To analyze this further, the disturbance terms also affect FF and FB type PQ control differently during the AC system fault event. Assuming an ideal inner current loop and v_q to be non-zero after an AC fault, according to the block diagram transfer functions shown before, we have:

FF type PQ control:

$$\frac{P^*}{v_d} \times v_{do} + v_q i_q = P, \quad \frac{Q^*}{-v_d} \times \left(-v_{do}\right) + v_q i_d = Q. \tag{12}$$

FB type PQ control

$$P^* \frac{skp_P v_{do} + ki_P v_{do}}{s\left(kp_P v_{do} + 1\right) + ki_P v_{do}} + v_q i_q \frac{s}{s\left(kp_P v_{do} + 1\right) + ki_P v_{do}} = P. \tag{13}$$

$$Q^* \frac{-skp_Q v_{do} - ki_Q v_{do}}{s\left(1 - kp_Q v_{do}\right) - ki_Q v_{do}} + v_q i_d \frac{s}{s\left(1 - kp_Q v_{do}\right) - ki_Q v_{do}} = Q. \tag{14}$$

It can be observed from the above equations that the disturbance terms $v_q i_q$ and $v_q i_d$ affect FF type control output power directly during the AC system fault event. However, they are attenuated in the case of FB type control by the outer controller. This is because FF type PQ control relies on the assumption that $P = v_d i_d$ and $Q = -v_d i_q$ which requires a correct operation of the PLL and is not able to "see" variations in v_q. FB type PQ controls are based on the fuller power equations and thus are able to modify their current references when the disturbance terms vary. A more comprehensive comparison of FF and FB type PQ controls is addressed in [22].

VI. Representative GB Test System

In this section, a test system based on a GB like reference case will be introduced. The characteristics found based on the generic two-area system will be further tested.

The test network takes a reduced order steady-state equivalent of the UK transmission system [11] and adds detailed models of generator, excitation systems, and Power System Stabilizers (PSSs). One aggregated generating unit is modeled at each generator bus, representing the dominant generation type at that bus. Different generation types (Fig.12), are parameterized with the corresponding dynamic data recommended in [23] to distinguish their dynamic behaviors. All generators in the system are represented by 6th order

synchronous generator models except the wind generator which is modeled as a connection converter with constant power factor control, representing a wind farm connected through a converter to the grid. Detailed wind turbine dynamics are not modelled since they are decoupled from the system by the converter [24]. Standard IEEE models of exciters are used for different generator types and PSSs are designed for each generator to damp local oscillatory modes. Standard IEEE exciters are used at for different generation types [25] and PSSs are designed for each generator to damp local oscillatory modes. A number of circumstances (e.g. different dispatch of generations, different loadings and etc.) may cause problems in such a system. To illustrate this, the paper has stressed the system further by adjusting the distribution of the load in different areas creating a situation that more power is transferred from the North to the South without any thermal branch overloads. This represents the situation that Scotland is exporting power for the heavy load demand in the England network, which will push the system to reach its stability margin with the total amount of 4GW power transferred in the onshore AC tie lines (6-9 and 8-10).

For a heavily stressed condition, the system model has a 0.47 Hz low frequency inter-area electromechanical mode [26]. Fig.13 highlights this unstable eigenvalue with damping ratio of -0.5%. The normalized right eigenvector, corresponding to rotor speeds, of inter-area mode, is also given in Fig.13 to show the grouping of generators in inter-area oscillation (mainly between G1-G4 and the rest of the generators). Based on the mode shape plot, an embedded VSC HVDC link is modeled, between bus 4 and 14, to connect the two generator groups. This represents a future eastern link proposed for the GB grid [27]. The power is transferred in the direction from VSC1 to VSC2 (North to South) with a total installed capacity of 1GW. The DC cables of approximately 400km are modeled using an appropriate number of lumped equivalent π sections.

There are in total more than 230 state variables in this integrated system which mainly includes the states in the synchronous generator models and controls, as well as the states in the VSC HVDC converters and controls. Due to the size of the whole integrated system, it is considered efficient to only calculate a specific set of eigenvalues with real and reactive part within the region of interest. The Arnoldi method is applied to solve and track the partial eigenvalues for the integrated system around a reference point with small negative real part and frequencies of 0.1-0.7Hz. The targeted critical modes are dominantly participated by the speed state variables in majority of the synchronous generators in the system. The focus is put on the damping ratio of the inter-area mode in this case. A series of tests are performed as listed in Table V with the resulting damping ratios calculated. Time domain simulations are also provided to support the eigenvalue analysis with a self-clearing 60ms three phase fault at bus24. This fault event also applies in the following simulation studies.

The test of comparing FF and FB type PQ controls in the VSC with different DC link operating conditions has been carried out in this case. Both types of PQ controls result in very similar inter-area mode damping with an increasing DC link power which is different from the case with the two area system before. As the AC system voltages are more stable due

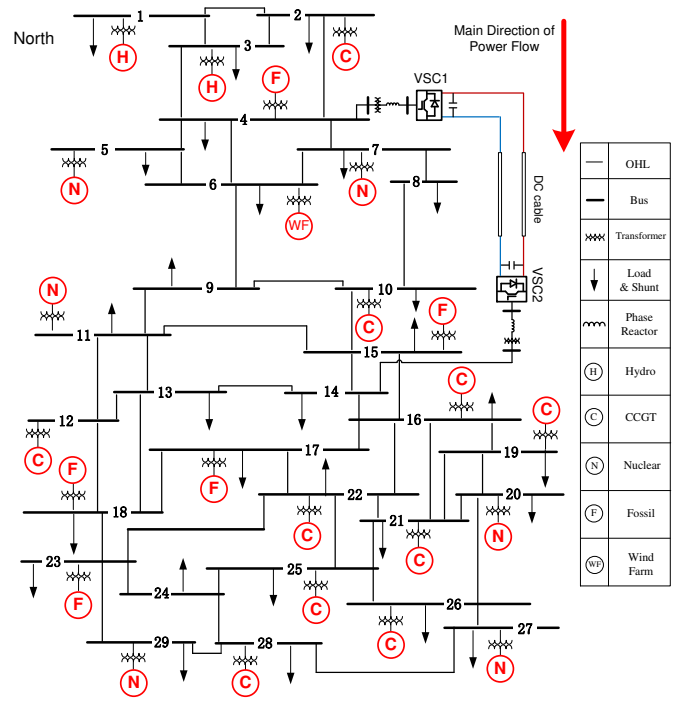

Fig. 12. "Dynamic GB system" with embedded VSC HVDC link.

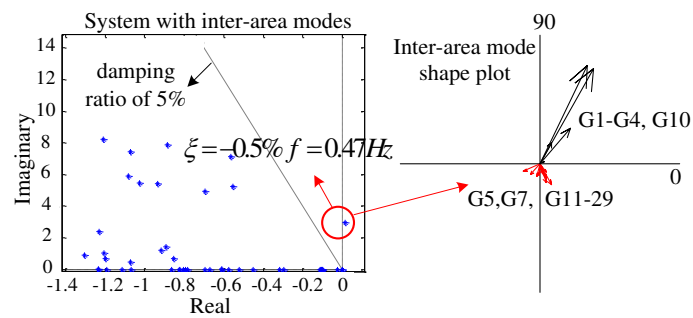

Fig. 13. Eigenvalues of the representative GB system (eigenvalues with small negative parts and positive frequencies only) and mode shape plot.

to the highly meshed nature of the representative GB system, the FF type PQ controls act in a manner equivalent to very fast FB type PQ controls. It is observed in Table V that the system moves from unstable (ξ *=-0.42%)* to marginal stable (ξ *=0.08%*) with increasing DC link power from 100MW to 900MW this time in both cases. Such results are validated in Fig.14 which compares the effect of FF and FB type controls as well as the effect of different DC link operating points on the tie line 8-10 power responses following the AC fault. It should be noted that, what would typically be considered a satisfactory damping (i.e. the resultant peak power deviation to be reduced fewer than 15% of its value at the outset within 20s) has not been achieved in this case.

As FBV_{ac} is found to have more impact on the inter-area oscillation than other VSC controls, a better and satisfactory damping effect may be achieved. The tracked inter-area mode damping ratios with FBV_{ac} in both VSCs of the DC link validate conclusion 3b before - A fast FBV_{ac} in the receiving area (VSC2) reduces the damping of the inter-area mode while a faster FBV_{ac} in the sending area (VSC1) improves the damping, as listed in Table V. This is further shown in the time

Table V Inter-area mode damping ratio for case studies in GB system

Test cases with control settings in test case 1	DC link power	Inter-area mode ξ %
FF and FB type controls	*100MW*	*-0.42%*
	500MW	*-0.15%*
	900MW	*0.08%*
Fast FBV_{ac} in VSC1	*500MW*	*3.12%*
Slow FBV_{ac} in VSC1	*500MW*	*-0.01%*
Fast FBV_{ac} in VSC2	*500MW*	*-0.51%*
Slow FBV_{ac} in VSC2	*500MW*	*-0.19%*

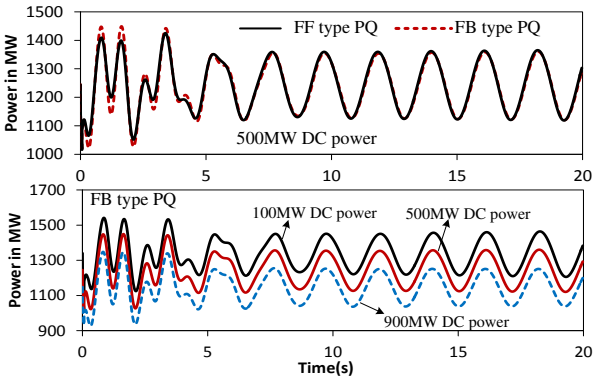

Fig. 14. Tie line 8-10 power responses with FF/FB type VSC control.

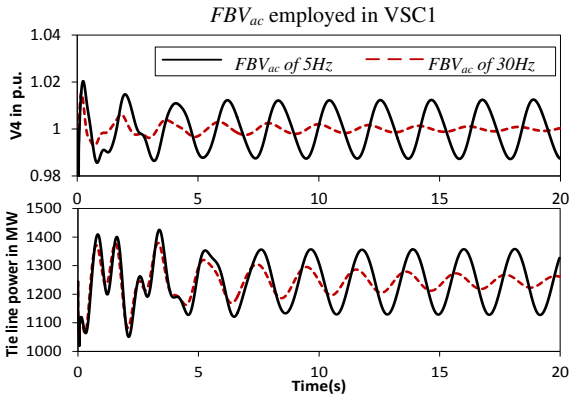

(a)

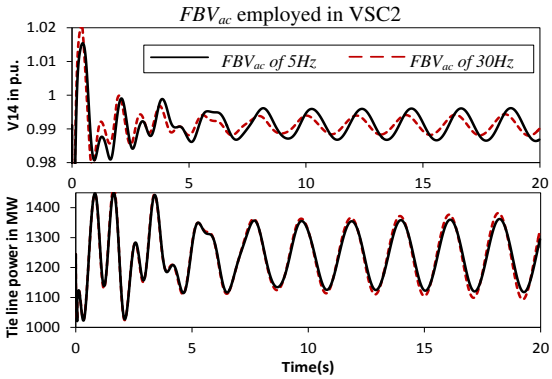

(b)

Fig. 15. (a) System Responses with FBV_{ac} control in VSC1. (b) System Responses with FBV_{ac} control in VSC2.

domain simulations for the AC fault in Fig.15. In both cases, the VSC controlled bus voltage is improved with faster FBV_{ac}. However, only a faster FBV_{ac} in VSC1 increases the system inter-area mode damping and thus stabilizes the post fault system. The opposite (though the effect is reasonably small) is seen when FBV_{ac} is employed in VSC2.

VII. Conclusion

A systematic comparison of the effects of VSC HVDC controls and operating conditions on the dynamic behavior of both AC and DC side of a system is provided, based on both generic two-area AC system and a realistic representative reduced order model of the GB transmission system. Modal analysis and transient simulations are used to study the AC and the DC side effects respectively. The conclusions of this study are applicable to both a standard theoretical two-area system and large realistic test system (GB system) and therefore provide useful insights and understanding of the possible influences brought by DC controls on the AC dynamics. The extent of this interaction and the full nature of it though, may vary from system to system depending on system structure and operating conditions and needs to be verified for any specific power system separately. These can be briefly summarized as:

The *operating point* of the DC link (power flow) and the *AC voltage control in VSCs* have larger influences on the AC system inter-area oscillation than other VSC controls. For an embedded VSC HVDC link (in parallel with AC tie lines), if FF type controls are used, it normally increases the damping of the inter-area mode at higher power flow. However, when FB type controls are used, its effects on the damping of inter-area mode may depend on the system structure.

Additionally, FBV_{ac} in the receiving area of an embedded VSC HVDC link with higher *bandwidth* reduces the damping of the inter-area mode while one in the sending area (VSC1) improves the damping. Varying the bandwidth of FBV_{ac} has less influence on the damping ratio of the inter-area mode at higher DC link power. However, the FBV_{ac} bandwidth variation has larger influence on the frequency of the inter-area mode at higher DC link power.

VIII. Appendix:

VSC HVDC link Model and Data: 1. Converter state equations:

$$L\dot{i}_d = -Ri_d + \omega L i_q + e_d - v_d$$

$$L\dot{i}_q = -Ri_q - \omega L i_d + e_q - v_q$$

$$\dot{V}_{dc} = -\left(\frac{e_d i_d + e_q i_q}{C_{eq} V_{dc}}\right) + \frac{I_{dc}}{C_{eq}}.$$

2. Controller and other equations:

$$e_d = k_d(i_d^* - i_d) + x_d - \omega L i_q + v_d$$

$$e_q = k_q(i_q^* - i_q) + x_q + \omega L i_d + v_q$$

$$\dot{x}_{dq} = \frac{k_{dq}}{T_{dq}}(i_{dq}^* - i_{dq}),\ \dot{x}_{outer} = k_{i_outer}(X^* - X)$$

$$i_{dq}^* = k_{p_outer}(X^* - X) + x_{outer}.$$

3. DC circuit equations:

$$C_{eq}\dot{V}_{dc1} = i_{dc1} - i_{dc}$$

$$C_{eq}\dot{V}_{dc2} = i_{dc2} + i_{dc}$$

$$L_{dc}\dot{i}_{dc} = V_{dc1} - V_{dc2} - R_{dc} i_{dc}$$

where x_{dq} and x_{outer} are the state variables in the current and outer controllers. X stands for V_{dc}, V_{ac} , P or Q for FB type controls. Other notations are presented in Fig.1 and Fig.4.

4. DC Lines parameters: R_{dc}=*0.0113 Ω/km*, L_{dc}= *0.466mH/km.*

5. Paralleled DC side equivalent capacitor is estimated as: $C_{eq} = 150\mu F$, operating at $\pm 320kV$.

6. Connection transformer T_c: *230kV/325.73kV* with short circuit voltage 15%.

7. Converter equivalent AC coupling phase reactor: $R=0.005p.u.$ $X=0.15p.u.$

IX. References

[1] N. Flourentzou, V. G. Agelidis, and G. D. Demetriades, "VSC-Based HVDC Power Transmission Systems: An Overview," *IEEE Transactions on Power Electronics,* vol. 24, pp. 592-602, 2009.

[2] T. M. Haileselassie and K. Uhlen, "Impact of DC Line Voltage Drops on Power Flow of MTDC Using Droop Control," *IEEE Transactions on Power Systems ,* vol. 27, pp. 1441-1449, 2012.

[3] L. Jun, J. Tianjun, O. Gomis-Bellmunt, J. Ekanayake, and N. Jenkins, "Operation and Control of Multiterminal HVDC Transmission for Offshore Wind Farms," *IEEE Transactions on Power Delivery,* vol. 26, pp. 2596-2604, 2011.

[4] X. Lie, Y. Liangzhong, and C. Sasse, "Grid Integration of Large DFIG-Based Wind Farms Using VSC Transmission," *IEEE Transactions on Power Systems,* vol. 22, pp. 976-984, 2007.

[5] Z. Lidong, L. Harnefors, and H. P. Nee, "Power-Synchronization Control of Grid-Connected Voltage-Source Converters," *IEEE Transactions on Power Systems ,* vol. 25, pp. 809-820, 2010.

[6] G. O. Kalcon, G. P. Adam, O. Anaya-Lara, S. Lo, and K. Uhlen, "Small-Signal Stability Analysis of Multi-Terminal VSC-Based DC Transmission Systems," *IEEE Transactions on Power Systems,* vol. 27, pp. 1818-1830, 2012.

[7] R. Preece, J. V. Milanovic, A. M. Almutairi, and O. Marjanovic, "Damping of inter-area oscillations in mixed AC/DC networks using WAMS based supplementary controller," *IEEE Transactions on Power Systems,* vol. 28, pp. 1160-1169, 2013.

[8] H. F. Latorre, M. Ghandhari, and L. Söder, "Active and reactive power control of a VSC-HVdc," *Electric Power Systems Research,* vol. 78, pp. 1756-1763, 2008.

[9] P. Kundur, *Power System Stability and Control*. London McGraw-Hill, Inc., 1994.

[10] K. R. W. Bell and A. N. D. Tleis, "Test system requirements for modelling future power systems," *IEEE Power and Energy Society General Meeting* , 2010, pp. 1-8.

[11] M. Belivanis and K. R. W. Bell, "Representative GB Network Model," Dep. of Electronic and Electrical Engineering, University of Strathclyde, Glasgow, 2011.

[12] N. R. Chaudhuri, R. Majumder, B. Chaudhuri, and P. Jiuping, "Stability Analysis of VSC MTDC Grids Connected to Multimachine AC Systems," *IEEE Transactions on Power Delivery,* vol. 26, pp. 2774-2784, 2011.

[13] "Guide for the Development of Models for HVDC Converters in a HVDC Grid," Cigre Working Group B4.57, 604, December 2014

[14] Z. Lidong, L. Harnefors, and H. P. Nee, "Modeling and Control of VSC-HVDC Links Connected to Island Systems," *IEEE Transactions on Power Systems,* vol. 26, pp. 783-793, 2011.

[15] C. Dierckxsens, K. Srivastava, M. Reza, S. Cole, J. Beerten, and R. Belmans, "A distributed DC voltage control method for VSC MTDC systems," *Electric Power Systems Research,* vol. 82, pp. 54-58, 2012.

[16] A. Kiam Heong, G. Chong, and L. Yun, "PID control system analysis, design, and technology," *IEEE Transactions on Control Systems Technology,* vol. 13, pp. 559-576, 2005.

[17] J. G. F. Francis, "The QR Transformation .2.," *Computer Journal,* vol. 4, pp. 332-345, 1962.

[18] Y. Saad, "Variations on Arnoldi's method for computing eigenelements of large unsymmetric matrices," *Linear Algebra and its Applications,* vol. 34, pp. 269-295, 1980.

[19] L. Wang and A. Semlyen, "Application of sparse eigenvalue techniques to the small signal stability analysis of large power systems," *IEEE Transactions on Power Systems,* vol. 5, pp. 635-642, 1990.

[20] J. Peralta, H. Saad, S. Dennetiere, J. Mahseredjian, and S. Nguefeu, "Detailed and Averaged Models for a 401-Level MMC HVDC System," *IEEE Transactions on Power Delivery,* vol. 27, pp. 1501-1508, 2012.

[21] M. Klein, G. J. Rogers, and P. Kundur, "A fundamental study of inter-area oscillations in power systems," *IEEE Transactions on Power Systems,* vol. 6, pp. 914-921, 1991.

[22] W. Wenyuan, A. Beddard, M. Barnes, and O. Marjanovic, "Analysis of Active Power Control for VSC HVDC," *IEEE Transactions on Power Delivery,* vol. 29, pp. 1978-1988, 2014.

[23] P. M. Anderson and A. A. Fouad, *Power System Control and Stability*, 2nd ed.: Wiley Blackwell , 2002.

[24] M. A. Poller, "Doubly-fed induction machine models for stability assessment of wind farms," presented at the Power Tech Conference Proceedings, IEEE Bologna, 2003.

[25] "IEEE Recommended Practice for Excitation System Models for Power System Stability Studies," *IEEE Std 421.5-2005 (Revision of IEEE Std 421.5-1992),* pp. 0_1-85, 2006.

[26] F. M. Hughes, O. Anaya-Lara, N. Jenkins, and G. Strbac, "A power system stabilizer for DFIG-based wind generation," *IEEE Transactions on Power Systems,* vol. 21, pp. 763-772, 2006.

[27] *Group Major Projects Status Update for Electricity Transmission* Available: https://www.gov.uk/government/groups/electricity-networks-strategy-group, December, 2014

X. Biographies

Li Shen (S'12) received the B.Eng. degree in the School of Electrical and Electronic Engineering in 2011 from The University of Manchester, U.K. and North China Electric Power University, China. Currently he is working towards the Ph.D. degree at The University of Manchester.

Mike Barnes (M'96–SM'07) received the B.Eng. and Ph.D. degrees from the University of Warwick, Coventry, U.K. In 1997, he was a Lecturer with the University of Manchester Institute of Science and Technology (UMIST, now merged with The University of Manchester), Manchester, U.K., where he is currently a Professor. His research interests cover the field of power-electronics-enabled power systems.

Robin Preece (GS'10, M'13) received his B.Eng. degree in Electrical and Electronic Engineering in 2009 and his Ph.D. degree in 2013, both from The University of Manchester, UK. He is currently a Lecturer in Power Systems Engineering at the same institution.

Jovica V. Milanović (M'95, SM'98, F'10) received his Dipl.Ing. and his M.Sc. degrees from the University of Belgrade, Yugoslavia, his Ph.D. degree from the University of Newcastle, Australia, and his Higher Doctorate (D.Sc. degree) from The University of Manchester, U.K., all in Electrical Engineering. Currently, he is a Professor of electrical power engineering, Deputy Head of School and Head of Electrical Energy and Power Systems Group in the School of Electrical and Electronics Engineering at The University of Manchester (formerly UMIST), U.K., visiting professor at the University of Novi Sad, Novi Sad, Serbia and conjoint professor at the University of Newcastle, Newcastle, Australia.

Keith Bell is the Scottish Power Professor of Smart Grids at the University of Strathclyde in Glasgow in the UK. He joined the University in 2005 having previously gained his Ph.D. at the University of Bath and worked as an electrical engineering researcher in Manchester and Naples, and as a system development engineer in the electricity supply industry in Britain. He is a Chartered Engineer, a co-Director of the multi-disciplinary UK Energy Research Centre (UKERC), and an invited expert member of CIGRE Study Committee C1 on System Development and Economics.

M. Belivanis received his MEng in Electrical Engineering from the University of Patras, Greece in 2007 and his M.Sc. from the University of Edinburgh, U.K. in 2008. He is currently working towards his Ph.D. degree at the Department of Electronic and Electrical Engineering at the University of Strathclyde in Glasgow, U.K.